Neutron resonance spectroscopy for $n+^{204}$Pb: Total and differential elastic scattering cross sections

R. F. Carlton
Physics & Astronomy Department, Middle Tennessee State University, Murfreesboro, Tennessee 37132

J. A. Harvey and N. W. Hill
Oak Ridge National Laboratory, Oak Ridge, Tennessee 37831

(Received 28 September 2002; published 4 February 2003)

We have measured the neutron total and elastic scattering cross sections for the ^{204}Pb$+n$ reaction over the neutron energy range 35–1000 keV. Neutron resonance widths and energies have been deduced for 1357 resonances from an *R*-matrix analysis of the total cross section data. Of this number 317, 424, and 617 are due to *s*-, *p*-, and *d*-wave interactions, respectively, with the parity assignments based mainly upon resonance asymmetries observed in the scattering data. The level densities and strengths of all partial waves are uniform up to a neutron energy of 500 keV. The *s*-, *p*-, and *d*-wave strength functions for this energy region are (in units of 10^{-4}) 1.3 ± 0.2, 0.19 ± 0.02, and 1.0 ± 0.1, respectively. If the strengths are calculated over the entire energy range the values for *s* and *d* waves are reduced by 35% and 12%, respectively, while that for *p* waves is increased by 40%. The *s*-, *p*-, and *d*-wave level densities (in keV^{-1}) are 0.33 ± 0.03, 0.44 ± 0.02, and 0.68 ± 0.01, respectively.

DOI: 10.1103/PhysRevC.67.024601 PACS number(s): 24.30.Gd, 25.40.Dn, 27.40.+z, 29.30.Hs

I. INTRODUCTION

A number of studies of the lead isotopes using neutron total, capture, and differential scattering cross sections have manifest both features to be expected in the region of a magic-number nucleus and departures from those expectations. A sudden onset of large *s*-wave strength in the neutron energy region of 40–500 keV has been reported for ^{206,207,208}Pb$+n$ and has been interpreted in the framework of doorway states [1]. Horen *et al.* [2,3], found evidence for *p*- and *d*-wave doorway structures in ^{206}Pb$+n$ through an analysis of differential scattering and total cross sections up to a neutron energy of 600 keV. They reported significant changes in the neutron strength function for *p*-wave neutrons at energies of 40 and 145 keV, which they attributed to doorway states arising from a $(d_{3/2}, 3^-)$ particle-core excitation. The *d*-wave strength function showed similar patterns near 425 keV for ^{206}Pb$+n$. Possible parity dependence in the level density in ^{207}Pb was also noted. Similar doorway structures have been reported [4,5] for ^{207}Pb$+n$ in the same energy interval and were similarly interpreted. A high-resolution study [6] of ^{204}Pb$+n$ over the neutron energy range 0–100 keV revealed distinctly different nuclear structure properties than the other lead isotopes. There were numerous, small *s*-wave resonances in this energy region which is well below the onset of large *s*-wave strength in ^{206,207,208}Pb$+n$. Furthermore, the *s*-wave strength was found to be more than a factor of 10 greater than that of these other isotopes in this limited energy interval. One could argue that comparison of strengths for an energy interval in one isotope (204) for which small *s*-wave strength and large doorway structures are seen in the other isotopes is not a convincing argument for the absence of doorway structures in ^{204}Pb $+n$. We have measured and analyzed higher-resolution differential scattering and total cross section data from the Oak Ridge Electron Linear Accelerator (ORELA). We have extended the neutron energy range of the analysis to 1 MeV and have identified spins and parities for 1357 resonances in this energy interval. We are thus able to examine the *s*-, *p*-, and *d*-wave strengths over the larger energy interval for a more realistic comparison with results of other isotopes of lead and consideration of the question of doorway structures in this isotope.

II. EXPERIMENT

A. Total cross section measurements

Neutron transmission measurements were performed at the Oak Ridge Electron Linear Accelerator facility, covering the energy region from 35 keV to 20 MeV. The accelerator was operated at 800 Hz at a power of 7 kW. The electron beam burst width was 3.25 ns. Collimators (1.35 cm in diameter) were used before and after the sample at 9 m such that only unmoderated neutrons from the Ta target reached the detector. Overlap neutrons were eliminated by a 0.3-g/cm^2 ^{10}B filter, and a 3.7-cm-thick uranium filter was placed in the beam to reduce the gamma flash from the target, both at 5 m. The neutron burst has a continuous energy spectrum from the photoneutron process in tantalum. The neutron energy resolution function is dominated, at the higher energies, by the burst width (3.25 ns), and the full width at half maximum for the 201-m flight path is given by

$$\left(\frac{\Delta E}{E}\right)^2 = (0.04 + 0.25E)\times 10^{-6},$$

where E is in MeV.

A rectangular NE-110 scintillator 5.2 by 8.9 cm in area and 2.5 cm thick was mounted between two RCA 8854 photomultipliers to form the detector which was located at a 201.575-m flight path. The detectors were gated off during the gamma flash and the succeeding ≈ 3 μs to eliminate extraneous events arising from phototube afterpulsing.

 ©2003 The American Physical Society

The two cylindrical samples totaled 92.7204 g with a diameter of 1.588 cm corresponding to a thickness of 0.1378 atom/b. However, the sample was enriched to only 71.41% ^{204}Pb with the ^{206,207,208}Pb impurity constituents representing 12.52%, 6.27%, and 9.78% of the sample, respectively. Hence, the magnitude of the impurity components was sufficiently large to warrant compensation through alternation, into and out of the beam, of a 0.3175-cm-thick sample of 88.33% ^{206}Pb plus a 1.001-cm-thick sample of natural Pb with the ^{204}Pb sample, all under computer control with a cycle time of approximately 20 min. However, this compensation slightly overcorrected for the ^{208}Pb. Since the ^{208}Pb resonance parameters are well known, a calculated correction was made for this overcompensation, resulting in an inverse sample thickness of Pb of 10.155 b/atom with ^{204}Pb representing 99.44% of the sample.

We used a neutron monitor to compensate for fluctuations in the neutron production rate during the measurements. Transmissions were counted for approximately 4 days over an 11-day period. Background determinations and optimization of signal to background ratio were facilitated by four separately recorded time-of-flight spectra corresponding to different pulse height biases. The overall background, for the energy analyzed, was $<1\%$. An EG&G time digitizer was used to acquire the data, and the resulting time-of-flight spectra were stored in the ORELA Data Acquisition Computers. The data were corrected for a dead time (1104 ns) in the digitizer and then for a constant room background. The transmission and total cross section were computed from the background-corrected sample-in–sample-out ratio, normalized to the same monitor counts.

B. Scattering cross section measurements

The scattering measurements also used the time-of-flight technique with neutron pulses from both the tantalum and the water-moderated parts of the ORELA target. The scattering measurements included a 0.3-g/cm^2 ^{10}B filter to eliminate low-energy neutrons associated with the previous burst and two other filters to reduce the intensity of the gamma flash from the target: a 0.73-cm-thick uranium filter covered the whole beam; the other, comprised of three 2.5-cm-thick layers of uranium, thorium, and tantalum, shadowed only the tantalum part of the target. Scattering data were collected for 270 h over a 4-week period. The burst rate of the accelerator was 800 Hz at a power level of 13 kW and the burst width was 6.5 ns. The neutron beam was collimated at 192 m, with both moderated and unmoderated neutrons reaching the scattering sample. The scattering sample was a 71.42-gm ^{204}Pb (71.41%) hollow cylinder 6.03 cm high, 3.175 cm inside diameter with a wall thickness of 0.122 cm. It was suspended in the center of a 1.83-m-diam evacuated scattering chamber at a distance of 200.191 ± 0.005 m from the neutron moderator. The scattering chamber was isolated from the neutron beam tube via a 0.025-cm Mylar window.

Six neutron detectors were located 19.1 cm from the center of the chamber at angles of 39°, 55°, 90°, 120°, 140°, and 160° from the direction of the incident neutron beam. Each neutron detector consisted of a 7.62-cm-long by 4.32-cm-diam cylinder of NE-110, viewed at each end by RCA 8850 photomultiplier tubes. The threshold for each phototube was set below the single photoelectron level, and a fast coincidence between the two tubes of each detector was required to define an event. The system was designed so that each detector could record a maximum of only one event from each accelerator burst (i.e., 800 s^{-1}). The data were corrected for dead time resulting from detection of the gamma flash scattered by the sample. One detector was placed in the direct beam, at reduced power, to measure the product of the flux and the detector efficiency as a function of neutron energy. A carbon scatterer was also used to intercalibrate the other five detectors and determine their energy efficiencies, relative to that of the detector placed in the direct beam. A neutron monitor detector was used to normalize all spectra. After correcting for dead time and a constant room background, the scattering spectra were divided by the spectrum from the direct-beam detector in order to remove the energy dependence of the incident flux and detector efficiency. The data were not corrected for multiple scattering in the sample. Additional details of the experimental arrangement for these scattering measurements can be found in the literature [7].

III. DATA ANALYSIS

We have employed an *R*-matrix analysis of the transmissions using the code SAMMY [8]. The channel radius used was 8.54 fm for each of the spin groups identified, fixed over the entire energy region of the analysis. The boundary condition was set equal to the shift factor at each resonance. The potential scattering contributions to the background cross section and the character of the interference between resonance and potential scattering was modeled through an external *R* function, for each spin group, as

$$R_{\ell J}^{\mathrm{ext}}(E) = \alpha_{\ell J} + \beta_{\ell J} E - \tilde{s}_{\ell J} \ln\left(\frac{E_{\mathrm{hi}} - E}{E - E_{\mathrm{lo}}}\right).$$

The parameters α and β are varied in the fitting process, and $\tilde{s}$ represents the average strength in the region outside that of the analysis and has been taken here to be the same as that within the analyzed region. E_{hi} and E_{lo} are the upper and lower energies of the analyzed region and have been set at 1000 and 0 keV, respectively. This function has been shown [9,10] to represent the contribution, within the analyzed region, from resonances outside that region and facilitates the modeling of average scattering functions with an optical model potential, to deduce the parameters of that potential. Both resolution broadening and a free-gas model [11] of Doppler broadening, using an effective nuclear temperature of 300 K, have been applied to the *R*-matrix theory for comparison to the experimental data. More details of the analysis approach can be seen in Ref. [12].

The total and scattering cross section data were analyzed in concert, the former to deduce the energies and widths of the resonances, and the latter to deduce the spins and parities of the associated levels. This required a fitting of the transmissions with an assumed spin and parity, followed by use of the resulting resonance parameters to calculate the differen-

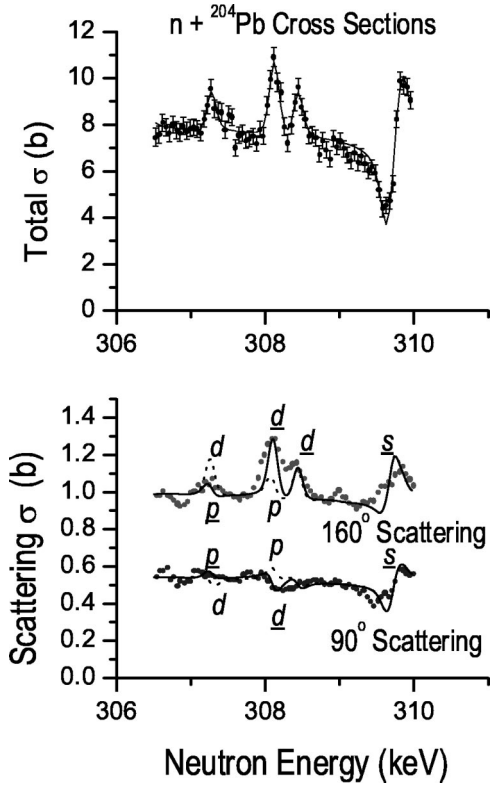

FIG. 1. Total and scattering cross sections for a selected energy region, to illustrate the manner of assigning resonance parities. The resonances are identified by parity, with the underlined symbols indicating the final assignment. The first two resonances had their parities swapped for the dashed curve. The solid curve is the scattering calculation for the assigned parities. Results for 160° offset by 0.5 b.

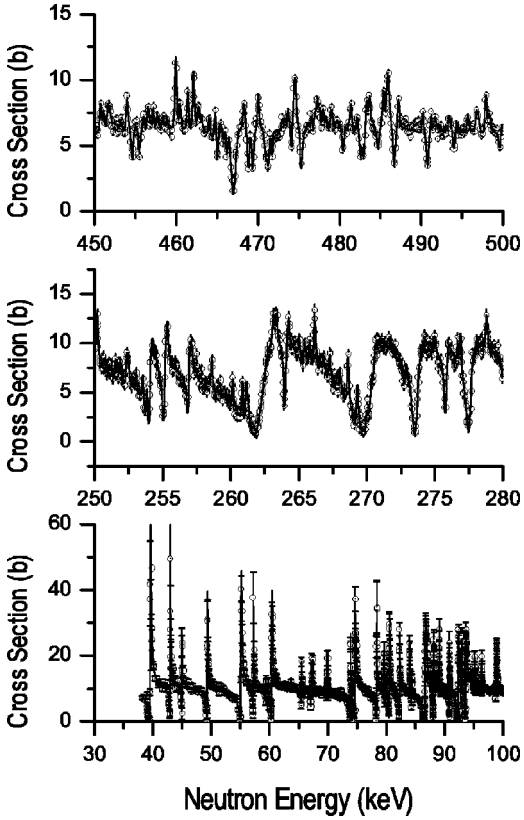

FIG. 2. Neutron total cross section of the ^{204}Pb+n reaction for selected energy regions, showing the changing character of the s-wave interactions with energy and their dominance throughout the spectrum. The symbols correspond to experimental measurements and the smooth curves to an R-matrix parametrization of the data. Symbols without error bars have errors less than the size of the symbols.

tial scattering cross section. The calculated scattering cross sections at each angle were used only to visually determine if the assumed spin and parity for a given resonance gave rise to the asymmetry differences observed among different scattering angles. Since the statistics of the scattering data were poor, judgments of which parity gave the better fit were based on which best represented the general trend of the prediction relative to the data and not whether the fit was even close in quality to that obtained in the total cross section data. The odd and even parities manifest very different asymmetries at forward and backward angles and thus served to permit the parity determination for most of the resonances. Figure 1 shows the total and elastic scattering cross sections for a selected neutron energy region to illustrate the manner in which the parity assignments were established from the scattering data. The p-wave interaction results in a more symmetric peak shape at 90°, and the d-wave manifests an asymmetry. The opposite is true, for each parity, at 160°. These scattering features have enabled parity assignments for resonances of comparable width and larger. The s-wave resonances are seen to be unambiguous in both total and scattering cross section data. For larger resonances the J value can also be deduced from the differing peak heights in the transmission data, for a given angular momentum. We thus have reasonably complete samples, by parity, for detected resonances but the J values are not reliable for the smaller resonances. With J^{π} assignments determined, the transmission data were fitted to obtain the final resonance parameters. We thus can report the strength functions and level densities for the s-, p-, and d-wave interactions.

IV. RESULTS

This study and analysis covers the energy range from 35 keV to 1 MeV. Three large s-wave resonances with energies (24.1, 27.5, and 32.8 keV) just below the beginning range of our data have been included in our resonance parameter file with their energies and widths held fixed at values taken from Ref. [13]. Representative energy regions of the total cross section are shown in Fig. 2, where the circles represent the data and the smooth curve the R-matrix representation of the data. Where no vertical bars are seen, the data uncertainties are smaller than the size of the symbols. The prominent s-wave resonances are seen throughout the energy ranges shown, those resonances being characterized by the dip in cross section resulting from resonance-potential scattering interference. This continues up to a neutron energy of 500 keV where the frequency of observed s-wave resonances begins to decrease somewhat. The gradual change in the shape of these resonances with energy can be seen in going from low to higher energies. The total cross section data are suf-

ficient to identify the *s*-wave resonances but not for the case of other partial waves. The elastic scattering data enable the determination of the parity of many of these resonances. The smaller non-*s*-wave resonances do not manifest sufficiently pronounced differences in their forward and backward asymmetries in the scattering data for different parities to permit the ℓ-value determination. Nevertheless, the parity is unambiguously determined for approximately 70% of the non-*s*-wave resonances up to 500 keV. For these resonances the spins in a given parity group are not unambiguously determined unless the peak cross section is such as to show the inadequacy of the smaller of the two spin possibilities. A total of 1357 resonances have been observed over the neutron energy range 35–1000 keV. The *s*-wave resonance parameters deduced from the analysis are presented in Table I. The uncertainties of the widths vary from approximately 5% for the larger resonances to 10% for the smaller ones with a minimum uncertainty of 0.5 eV. Energy uncertainties as given above in the experimental details vary from 0.02% at 50 keV to 0.05% at 1 MeV. The full list of resonances, including the other partial waves, has been sent to the Brookhaven National Nuclear Data Center. The parameters for the external *R* functions are given in Table II. These functions are an essential part of the *R*-matrix representation of the data, making it possible to account for the resonance-potential scattering influence of unobserved resonances outside the region of analysis without having to use a different channel radius for each spin group. Another alternative is to use combinations of resonances outside the region, called ''poles,'' to provide the necessary interference patterns.

In the following discussion of the results, two values of deduced average quantities are given. The first is based upon an upper energy of 500 keV and the second, presented in parentheses, is based upon an upper energy value of 1000 keV.

A. *s* waves

We observe a total of 186 (317) resonances over the energy region up to 500 keV (1000 keV). The *s*-wave strength function for ^{204}Pb+*n* is represented by the slope of the plot of the cumulative neutron width as a function of energy, as plotted in Fig. 3(a). The result is $1.3\pm0.2\times10^{-4}$ ($0.85\pm0.07\times10^{-4}$). The level density, shown in Fig. 3(b), is seen to be uniform up to an energy of 500 keV. We have not corrected for missing resonances but have chosen, rather, to calculate the strength functions and level densities based upon upper energies of both 500 keV and 1000 keV. The level density is determined, from the slope of the cumulative number of resonances plotted as a function of neutron energy, to be 0.40 ± 0.02 keV^{-1} (0.33 ± 0.01 keV^{-1}). We find 23 *s*-wave resonances between 35 and 100 keV, in agreement with Ref. [6]. In the energy range 0–100 keV that study reported 38 *s*-wave resonances, due to their increased sensitivity to low-energy resonances. This number of *s*-wave resonances stands in striking contrast to the number observed, in this energy range, for ^{206,207,208}Pb of 3, 1, and 0, respectively.

Rather complete neutron total cross section data are now available for the ^{204,206,207,208}Pb isotopes and reveal very different numbers of *s*-wave resonances (186, 17, 13, and 1, respectively, up to a neutron energy of 550 keV). An even more interesting feature of the variation of the neutron-nucleus interaction, with proximity to the $N=126$ closed neutron shell, is clearly manifest for *s*-wave resonances in Fig. 4 which shows the cumulative sum versus energy of the reduced width multiplied by the spin statistical factor *g*. The *s*-wave neutron strengths, given by the slopes of these histogram plots over the energy range for which resonances are observed, are seen to increase as one approaches the closed neutron shell. For each isotope there are regions where the cumulative sum increases more dramatically, over a narrow energy interval, with the spacing between those increases, increasing with closed-shell proximity. Such sudden increases in the cumulative sums have been interpreted as doorway states in the entrance channel, resulting from particle-core interactions. In the absence of background states with which to mix, the doorway would appear as an isolated resonance as in the case of ^{208}Pb. As the number of background states increases, mixing would give rise to spreading of the doorway more broadly over the continuum. While the data for all the investigated isotopes of lead certainly suggest increasing spreading of the doorway, the latest data for ^{204}Pb suggest that any doorway state is by now highly fragmented, and the number of background mixing states is sufficiently large so as to render the vestiges of doorway structures rather dim. This is seen in the barely discernable enhancements of the cumulative sum at neutron energies of 180, 260, 340, and 430 keV in Fig. 3.

Since the *s*-wave resonance structure dominates the spectrum, with all other resonances superimposed on that major structure, we have only presented the parameters for the *s*-wave resonances in Table I.

B. *p* and *d* waves

We have identified a total of 204 (424) and 283 (617) *p*-wave and *d*-wave resonances, respectively. The plot of cumulative neutron width as a function of neutron energy for *p* and *d* waves is shown in Fig. 3(a). By plotting the quantity $\Sigma g\Gamma_n^\ell/(2\ell+1)$ versus the neutron energy, where ℓ is the orbital quantum number, the strength is given simply by the slope of the graph. Here we see an absence of any structure suggestive of doorway states, the same being true for the corresponding level density plots, shown in Fig. 3(b). The strength functions are (in units of 10^{-4}) 0.19 ± 0.02 (0.27 ± 0.02) and 1.0 ± 0.1 (0.88 ± 0.05) for *p* and *d* waves, respectively, where the uncertainty is calculated from $[2.27/(n-1)]^{1/2}S^\ell$, with *n* the number of resonances.

The level densities due to *p*- and *d*-wave interactions are (in keV^{-1}) 0.45 ± 0.02 (0.44 ± 0.01) and 0.70 ± 0.02 (0.68 ± 0.01), respectively. For the *p*- and *d*-wave groups the cumulative reduced width plots suggest possible missing strength for *d* waves and enhanced strength for *p* waves above 700 keV. Rather than being due to misassignment of the parity, this suggests structure effects. The integrity of the parity assignments is quite good below 500 keV, and thus the deduced strengths, based upon that upper energy, have greater confidence. The differences between the level densi-

TABLE I. The ^{204}Pb+n R-matrix s-wave resonance parameters deduced from transmission and scattering analyses.

Energy (keV)	Γ_n (eV)	Energy (keV)	Γ_n (eV)	Energy (keV)	Γ_n (eV)	Energy (keV)	Γ_n (eV)
39.542	149.5	270.191	1436.2	442.332	213.8	669.503	146.8
42.962	46.9	272.787	22.7	443.765	36.3	673.285	35.9
44.938	20.5	273.681	536.5	446.242	71.5	675.764	196.3
49.319	53.2	275.82	120.6	448.651	36.4	677.224	73.3
55.098	153.6	277.6	461.4	448.93	258.7	680.199	454.1
57.214	35.3	280.13	91	449.35	645.1	687.16	61
59.294	4.9	282.465	31.8	454.64	97.8	692.7	50.7
60.37	91.5	285.136	97.5	455.49	70.1	694.378	120.9
65.453	10.5	285.961	35.5	465.055	69.4	700.133	144.7
66.153	2.1	288.69	263.6	466.332	100.1	705.024	196.3
67.114	14.5	290.919	851.4	467.072	610.6	706.416	222
73.852	41.5	292.528	180	468.868	140.3	713.119	155
74.64	144	293.371	63.9	469.363	164.4	713.34	270.7
78.322	75	297.077	23.3	470.986	69.1	717.114	45.6
80.503	59.8	297.441	105.6	471.235	142.9	718.97	67.6
82.235	54.1	299.701	42.8	471.69	78	721.708	40.9
84.334	8.5	303.833	25	474.148	240.8	724.843	36.9
86.676	251.7	305.659	52.2	475.301	162.4	729.964	41.6
88.073	41.6	309.677	70.1	480.395	70.6	732.965	280.8
90.799	26.6	312.595	196.4	482.603	76.7	737.466	158.2
92.342	144.1	315.436	31.2	482.917	77.3	739.775	70
93.6	140.7	317.305	40.2	484.699	55.1	747.935	57.9
100.919	8.5	319.257	62	486.707	136.7	751.474	72.6
101.951	31.8	320.783	15.3	490.783	109	754.785	209.2
103.541	69.4	326.035	375	494.039	48.7	758.868	80.4
110.503	9.3	328.148	252.1	499.645	40.1	764.98	232.8
116.024	238.1	330.847	46.6	504.566	84.8	766.506	44.7
119.012	70.2	332.167	317.4	505.172	224	768.373	70.7
124.378	187.3	333.162	212.2	509.976	17.7	772.339	43.9
127.046	8.4	333.549	252.3	516.59	56.9	777.644	115
134.116	257.6	336.956	87.7	517.657	122.7	784.58	149.8
136.821	223.9	340.48	236.4	522.427	73.5	796.589	75.6
135.011	62.9	340.681	151.3	523.214	48.2	798.107	351.3
140.063	119.5	342.6	9.1	526.141	138	799.895	79.3
141.584	2.5	342.839	525	526.653	110	804.725	142.8
143.317	4.8	345.952	280.6	528.279	114.1	807.213	57.7
143.57	31.1	349.317	789.4	530.546	105.5	808.381	40.1
146.212	218.5	352.236	430.6	531.905	30.6	809.532	75.4
147.691	48	353.159	212.9	535.229	195.3	814.145	760.6
148.928	251.2	354.861	138.6	536.579	447.6	817.782	290.9
153.091	108.3	359.111	43.9	539.334	206.5	820.636	184.6
155.407	7.2	360.383	32.5	543.841	132.2	823.91	419.4
158.745	72.2	360.583	193.5	546.126	280.1	829.485	571.2
161.217	116.4	360.916	119.8	547.909	28.9	834.637	87
164.852	27.7	364.454	177.9	549.248	392.4	836.699	426.3
166.539	162.7	366.247	119.1	550.683	57.1	839.931	126.4
168.017	69.6	370.011	56.2	552.346	63.5	841.043	78.9
170.795	51.1	375.031	97.7	554.184	145.5	848.821	40
172.54	2	376.44	11.3	567.6	28.7	853.614	71.7
173.274	2.3	376.954	61.6	570.6	39.5	866.914	356.5
174.789	82.2	378.685	20.9	575.95	23.5	867.647	92.2

TABLE I. (*Continued*).

Energy (keV)	Γ_n (eV)	Energy (keV)	Γ_n (eV)	Energy (keV)	Γ_n (eV)	Energy (keV)	Γ_n (eV)
176.156	229	380.061	36.1	582.792	25.6	873.744	69.8
178.265	427.7	381.27	97.9	584.887	26.3	877.75	274.6
181.49	116.3	386.632	69.3	586.276	64.2	880.121	207.8
185.595	329.2	390.556	305.8	587.759	184.1	892.117	78.7
187.437	1205.1	392.714	142.5	594.389	116.3	898.296	60.1
188.025	108.4	393.325	90.4	598.017	56.3	902.073	48.2
191.835	20.1	395.433	88.3	598.915	36	907.223	92.9
194.799	219.8	397.96	313	601.986	69.9	908.4	37.6
199.288	127	400.466	26.7	603.576	126.7	917.201	302.4
202.794	68.1	404.027	23.6	605.164	69.7	920.236	89.3
203.179	7.7	406.386	18.6	607.111	22.5	926.54	50.6
205.63	145.5	406.784	212.3	608.55	88.4	934.174	113.8
206.407	201.4	408.256	216.1	609.632	42.6	945.665	621.1
209.78	273.5	410.269	19.1	610.678	55.7	949.454	432.1
214.544	6.3	410.521	67.9	615.844	167.4	950.308	12.8
218.773	825.7	413.568	11.8	625.799	119.1	954.082	63.2
221.312	67.9	417.69	67.7	627.852	25.4	955.308	99.5
224.972	130.7	418.032	243.5	634.475	111.7	957.156	125.4
230.564	131	418.933	77.4	635.348	36.1	958.509	55.8
234.629	142.5	421.108	20.1	638.538	37.4	966.116	143.2
238.735	108.8	422.139	30.3	642.094	123.8	968.149	108.8
242.309	65.8	425.519	202	643.135	291	987.458	68.5
246.073	31.5	428.798	95.2	644.168	85.1	991.319	85.6
247.829	651.9	431.336	1156	645.002	32.3	993.443	33.8
254.044	272.6	433.117	397.7	645.9	94.1	995.514	101.5
255.116	119.3	436.307	63.7	649.678	159.6	996.799	71.5
256.894	67.3	437.796	181.4	652.499	148.3		
262.231	1579.3	439.426	39.5	653.487	481.8		
263.99	116.8	440.598	573.9	661.303	280.8		

ties for the different energy ranges are minimal, reflecting the uniformity of levels throughout the entire energy region. The d/p level density ratio (1.5 ± 0.1) is in reasonable agreement with the value expected on the basis of statistical considerations (1.7) while that for the p/s level density ratio (1.3 ± 0.1) differs significantly from the expected value of 3.0.

TABLE II. Parameters of the external R function for all observed partial waves.

J^π	α	β ($\times 10^4$ keV^{-1})	$\tilde{s}$
$\frac{1}{2}^+$	-0.117(6) [a]	1.55(8)	0.022
$\frac{1}{2}^-$	-0.078(6)	0.18(4)	0.005
$\frac{3}{2}^-$	-0.28(1)	0.44(8)	0.010
$\frac{3}{2}^+$	-0.03(1)	0.0	0.068
$\frac{5}{2}^+$	-0.006(5)	0.0	0.007

[a]In our notation 0.117(6) means 0.117 ± 0.006, etc.

V. CONCLUSION

The (almost) uniform strength and level density for (s), p, and d waves, as a function of neutron energy, suggest that doorways play a much less significant role for $^{204}\mathrm{Pb}+n$, compared to neighboring isotopes of lead. Before the data on s-wave strength in lead isotopes were complete, some investigators reported s-wave strengths among the various isotopes that differed by as much as an order of magnitude, in disagreement with systematic trends of the s-wave strength function in this mass region. In ^{208}Pb, for example, virtually all the s-wave strength is seen in a single resonance at 512 keV while in ^{204}Pb most of the strength is spread over the neutron energy range (0–1000 keV). From Fig. 4 the total sum of reduced neutron widths (and thus the strength) is seen to be essentially the same for all isotopes, up to 550 keV. In that regard it is worth noting that the additional s-wave strength observed in ^{204}Pb between 500 and 1000 keV gives a strength function for this isotope (over the energy range 0–1000 keV) that is in agreement with the others, calculated over the 0–550 keV interval. This corroborates the suggestion that the doorway states for ^{204}Pb are highly fragmented

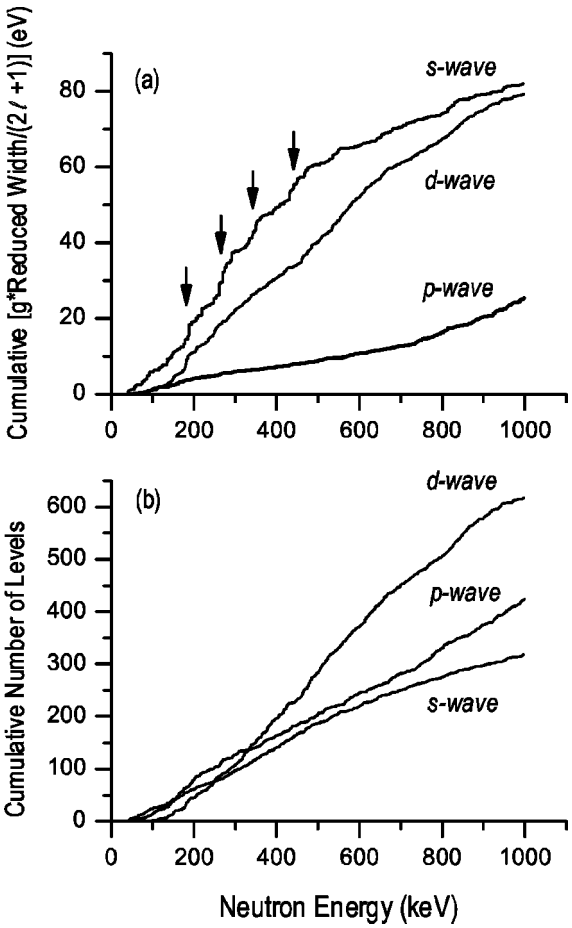

FIG. 3. (a) The cumulative reduced neutron width and (b) the cumulative number of levels versus neutron energy. The slope of (a) gives the strength and that of (b) gives the level density. Arrows indicate regions of increased strength.

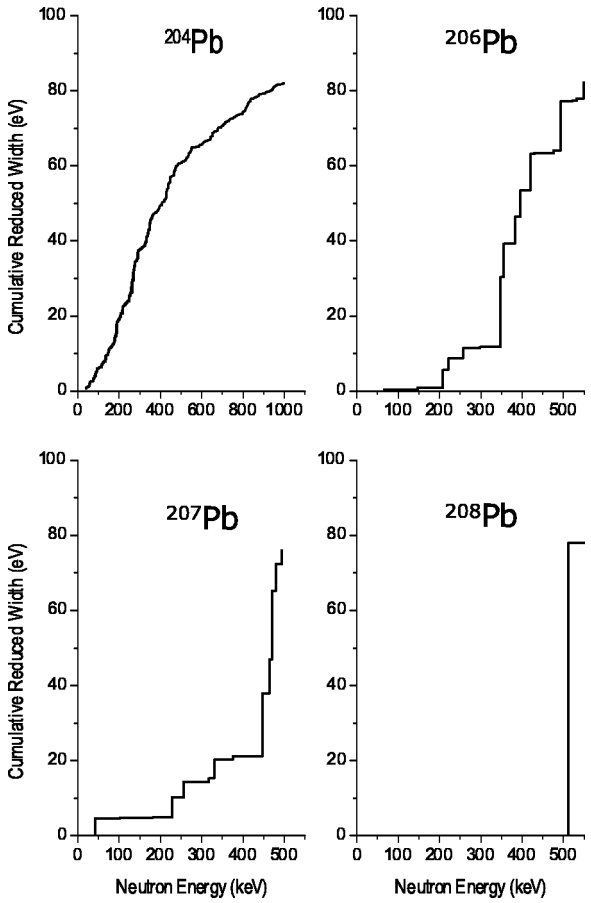

FIG. 4. *s*-wave cumulative reduced neutron width versus neutron energy for the stable isotopes of lead, demonstrating the trend of sudden increases as the closed $N=126$ shell is approached but yet the approximately similar total strengths in the 0–550 keV energy interval.

and that the strength of the neutron interaction is spread over a larger energy interval for this isotope. Though the parity groupings established in this study may not be completely unambiguous, changes in the strength and level density trends that would result if changes were made in some of the subjective assignments would not be such as to produce the type of large step increases in either the strength functions or level spacings that has been reported for the other isotopes of lead, for any of the partial waves. It has been conjectured [6] that this could be due to the fact that the doorway state is completely mixed with the background states or that ^{204}Pb must be sufficiently removed from the doubly magic core that the particle and phonon excitations that would give rise to any doorways are highly fragmented. The strength functions deduced from this study are consistent with general trends in this mass region, and differences with respect to other lead isotopes are likely a result of differing nuclear structure effects.

ACKNOWLEDGMENTS

This research was sponsored by the Basic Energy Sciences Division of the U.S. Department of Energy under Contract No. DE-FG05-86ER40293 with Middle Tennessee State University. Oak Ridge National Laboratory is managed by UT-Battelle, LLC for the U.S. Department of Energy under Contract No. DE-AC05-00OR22725.

[1] R. Kohler, J. A. Wartena, H. Weigman, L. Mewissen, F. Poortmans, J. P. Theobald, and S. Raman, Phys. Rev. C **35**, 1646 (1987).

[2] D. J. Horen, J. A. Harvey, and N. W. Hill, Phys. Rev. C **20**, 478 (1979).

[3] D. J. Horen, J. A. Harvey, and N. W. Hill, Phys. Rev. C **24**, 1961 (1981).

[4] D. J. Horen, J. A. Harvey, and N. W. Hill, Phys. Rev. Lett. **38**, 1344 (1977).

[5] D. J. Horen, J. A. Harvey, and N. W. Hill, Phys. Rev. C **18**, 722 (1978).

[6] D. J. Horen, R. L. Macklin, J. A. Harvey, and N. W. Hill, Phys. Rev. C **29**, 2126 (1984).

[7] D. J. Horen, C. H. Johnson, J. L. Fowler, A. D. MacKellar, and

B. Castel, Phys. Rev. C **34**, 429 (1986).
[8] N. M. Larson, Technical Report No. ORNL/TM-9179/R6, Oak Ridge National Laboratory, 2002.
[9] C. H. Johnson, C. Mahaux, and R. R. Winters, Phys. Rev. C **32**, 359 (1985).
[10] C. H. Johnson and R. R. Winters, Phys. Rev. C **21**, 2190 (1980).
[11] N. M. Larson, M. C. Moxon, L. C. Leal, and H. Derrien, Technical Report No. ORNL/TM-13525, Oak Ridge National Laboratory, 1998.
[12] R. F. Carlton, R. R. Winters, C. H. Johnson, N. W. Hill, and J. A. Harvey, Phys. Rev. C **38**, 1605 (1988).
[13] S. F. Mughabghab, *Neutron Resonance Parameters and Thermal Cross Sections* (Academic Press, Orlando, 1984), Pt. B, Vol. 1.